Flow Optimization of a MVHR combined with an Exhaust air Heat Pump by means of CFD Simulation

Fabian Ochs[1], Marco Romani[2], Michele Bianchi Janetti[1]
1. Unit for Energy efficient Building, University of Innsbruck, Innsbruck, Austria
2. Cetra Air Handling Units, Galletti Group, Altedo, Italy

Abstract
A simplified methodology to model and optimize a ventilation system is presented. A CFD model of a compact MVHR is developed with COMSOL Multiphysics® CFD Module, and an optimization method based on standard deviation is used to compare flow homogeneity of different supply duct geometries. Results encourage further development.

Introduction
In the framework of the research project "SaLüH!" a compact mechanical ventilation heat recovery system (MVHR) with integrated micro-heat pump was developed. The aim was to obtain a high level of prefabrication combined with a compact design allowing for installation also in small flats, e.g. into the façade. Due to the compactness, the system must be optimized as far as pressure drop, flow homogeneity and sound emissions are concerned [1].
This paper investigates the preliminary CFD modelling and optimization of the system, concentrating on the supply air duct. The aim was to analyze and compare the inlet air flow homogeneity in front of a straight and V-styled condenser.
The model assumes isothermal, incompressible flow through the duct. A 2D heat exchanger models was calibrated with respect to pressure drop and inlet velocity profile. A preliminary comparison with experimental data is carried out for both pressure drop and 2D transitional flow around a bluff body, by employing respectively EES – Engineering equation solver - and the measures of Lourenco and Shih for the near wake of a circular cylinder at Re = 3900, reported in [2]. Hence, four different 3D models are compared. A homogeneity coefficient based on standard deviation is introduced and calculated for the normal velocity component to the condenser inlet surface. The results show that a very compact system can result in a lack of homogeneity of the air flow through the heat exchangers, which can only be slightly reduced by splitting the condenser in two parts.

MVHR description and modelling
Compact MVHR for residential applications have a complex inner structure. Although the casing is a simple parallelepiped, the internal airflow weave through a tortuous 3D layout of finned heat exchanger, plate heat exchanger, centrifugal fan, piping, compressor and other components (Figure I)

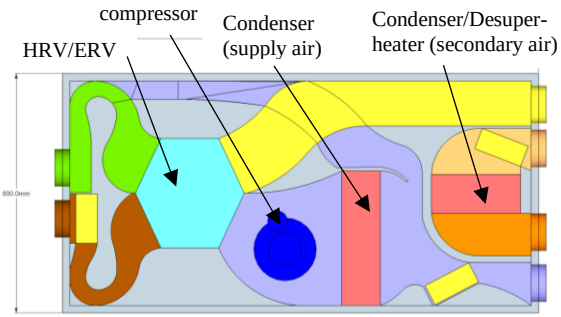

Figure I Scheme of compact MVHR combined with integrated micro heat pump (concept, FFG project SaLüH!) with compressor positioned between MVHR and condenser.

Within the supply air duct, the air flows out of the counterflow plate heat exchanger and encounter the body of the compressor. At the end of the duct enters the finned tube heat exchanger structure.
The CFD modelling and optimization of this structure is challenging under the computational point of view [3]: hence, a simplified modelling methodology is established.

Geometric models
Reference geometry is based on the functional model of the concept developed within the project EU "iNSPiRE" [4] and further developed in the FFG project SaLüH!. Dimensional constraints are given by the size of the condenser and the compressor. Four different configurations are compared, depending on whether the fan is placed upstream or downstream the condenser (Tab. I, Fig. II).

Fan: downstream		Fan: upstream	
Conf.1	Reference configuration without compressor	Conf.3	Split configuration: higher frontal area of the condenser
Conf.2	Reference configuration with compressor	Conf.4	Split configuration: Reference frontal area of the condenser

Table I. Supply duct configurations.

Four different distances between the compressor vertical axis and the condenser are also examined (15, 19, 23, 26 [cm]) Condenser volume is kept constant among the four geometries, in order to maintain the heat exchange surface of the reference configuration. Velocity field homogeneity in front of the heat exchanger is then compared and analysed.

The presence of the fins and the pressure drop through the heat exchanger can have an influence on the velocity field upwind and must be taken into account in the simulation. The tortuosity of this system make the use of a porous media fluidynamic model straightforward [5][6].
The rotary compressor can be considered a cylindrical bluff body characterized by a short aspect ratio (height/diameter). Complex vortex structures characterize the internal flow past this obstacle, where a strong interaction between the wake, the MVHR panels and the condenser take place.

$\dot{V}$	100	$[m^3/h]$
T_{in_duct}	18	$[°C]$
$T_{out\ duct}$	42.5	$[°C]$
P_{out_duct}	101325	$[Pa]$
ρ_{in}	1.213	$[kg/m^3]$
μ_{in}	1.811 e-5	$[Pa \cdot s]$
$D_h = 4S/P$	277.6	$[mm]$
$v_{in} = \dot{V}/S$	0.345	m/s
$\nu = \mu/\rho$	$1.493 \cdot 10^{-5}$	$m^2/s]$
$Re = (v_{in}\, D_h)/\nu$	6414	

Table II. Boundary conditions and model parameters

Boundary conditions suggest that the flow inside the supply air duct is not fully turbulent. Particular care is given to the choice of the turbulence model.

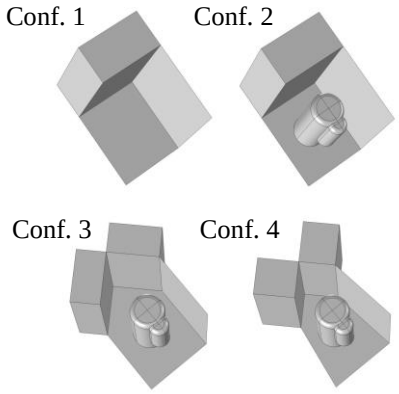

Figure II. Casing configurations

Numerical Model and Governing Equations

Momentum transport equation for incompressible and isothermal flow are solved using COMSOL Multiphysics® CFD Module. Two physics interfaces are coupled.

In the free flow domain RANS are solved to obtain velocity and pressure field..

$$\left(\frac{\partial\langle \mathrm{u_i}\rangle}{\partial \mathrm{t}} + \langle \mathrm{u_i}\rangle\frac{\partial\langle \mathrm{u_i}\rangle}{\partial \mathrm{x_j}}\right) = -\frac{1}{\rho_0}\frac{\partial\langle \mathrm{P}\rangle}{\partial \mathrm{x_i}} + \frac{\partial}{\partial \mathrm{x_j}}\left[(\nu + \nu_\mathrm{T})\left(\frac{\partial\langle \mathrm{u_i}\rangle}{\partial x_j} + \frac{\partial\langle \mathrm{u_j}\rangle}{\partial \mathrm{x_i}}\right)\right] + \frac{1}{\rho_0}\mathrm{F_i}$$

In the heat exchanger domain, Brinkman Equations are solved. In Einstein notations it reads:

$$\frac{1}{\varphi}\left(\frac{\partial \bar{u}_\mathrm{i}}{\partial \mathrm{t}} + \mathrm{u_j}\frac{\partial \bar{u}_\mathrm{i}/\varphi}{\partial \mathrm{x_j}}\right) = -\frac{1}{\rho_0}\frac{\partial \mathrm{P}}{\partial \mathrm{x_i}} + \frac{\partial}{\partial \mathrm{x_j}}\left[\frac{\nu}{\varphi}\left(\frac{\partial \bar{u}_\mathrm{i}}{\partial x_j} + \frac{\partial \bar{u}_\mathrm{j}}{\partial \mathrm{x_i}}\right)\right] + \frac{1}{\rho_0}\mathrm{F_i}$$

where

$$F_i = -\left(\sum_{j=1}^{3}\frac{\mu}{K_{ij}}\bar{u}_j + \sum_{j=1}^{3}\frac{C_F\rho}{\sqrt{K_{ij}}}|\bar{u}|\bar{u}_j\right)$$

is the Brinkman Equations specific force term, that takes into account permeability, viscosity and a form-drag-coefficient[1].
The second order term coefficient is called Forchheimer drag coefficient and takes into account inertial drag effect, that comes into play for fast flows through large pores [7]

$$\frac{C_F\rho}{\sqrt{K_{ij}}}|\bar{u}|\bar{u}_\mathrm{j} = \beta_{\mathrm{Fij}}|\bar{u}|\bar{u}_\mathrm{j}$$

Boussinesq viscosity model

Compressor cilindrical gometry leads to a pressure-driven boundary layer detachement. The choice of the most appropriate closure equation system is made by

[1] In COMSOL Multiphysics® the form drag coefficient is one–dimensional by default. In the framework of this paper work, the Forchheimer drag coefficient is isotropic, even though a user-customized Forchheimer tensor could be defined.

employing a standard benchmark in CFD: the flow past a cylinder in the sub-critical *Schiller-Linke* regime [2]. In this regime the boundary layer's transition to turbulence takes place in the free shear layer after the bluff body, and not at the wall surface.
COMSOL Multiphysics® CFD Module offer six different Boussinesq viscosity models (BVM). Standard k-ε, k-ω and AKN k-ε and SST k-ω are compared for their ability to predict wake length and kinetic turbulent energy production in the free shear layer.
Simulations results are compared with experimental data[2] .

Momentum sink term

The pressure drop along the heat exchanger must be predicted correctly. Moreover, the effect of the fins must be taken into account. A calibration of the model envisages the calculation of the Forchheimer drag coefficient and the permeability scalar contained in the momentum sink term. The methodology described in Musto et alii. is employed. A second order polynomial curve (pressure as a function of velocity) is calculated in EES – Engineering Equation Solver – for a reference heat exchanger model (scf-872c). The first and second order polynomial coefficients are used to obtain the momentum sink term of Brinkman Equations by solving the following equation system.

$$\begin{cases} \dfrac{\Delta P}{\Delta x} = a \cdot \vec{u} + b \cdot \vec{u}^2 \\ \dfrac{\vec{F}}{\Delta x} = \dfrac{\mu}{K}\vec{u} + \left(\dfrac{\rho C_F}{\sqrt{K}}\right)\vec{u}^2 \end{cases}$$

In COMSOL Multiphysics®, the permeability tensor is referred to Cartesian coordinates. In this paper the tensor is modified in such a way that the velocity field resembles the presence of the fins. By this way, within the heat exchanger domain only the velocity component normal to the inlet surface is preserved. The resulting equation to be solved inside the condenser domain is

$$\frac{\partial P}{\partial x} = -\sum_{j=1}^{3} \frac{C_F \rho}{\sqrt{K_{xj}}} |\bar{u}| \bar{u}_x$$

When the V-styled condenser is modelled, one branch is directed along the x-axis and the other branch along the y-axis, in order to avoid non-physical results. The permeability tensor for these branches reads respectively for the x and y axis:

$$K_x = \begin{pmatrix} K_{xx} & 0 & 0 \\ 0 & b_y & 0 \\ 0 & 0 & b_z \end{pmatrix}$$

$$K_y = \begin{pmatrix} b_x & 0 & 0 \\ 0 & K_{yy} & 0 \\ 0 & 0 & b_z \end{pmatrix}$$

b_x, b_y, b_z are o(K) values.

Optimization methodology

Only the velocity component *normal to the condenser inlet surface* is considered, i.e. the only component which is transported through the simplified condenser and participates in mass transport. All the measurements are taken on a *test surface* which is 1 cm far from the condenser surface [1]. The parameter used to compare the different supply duct configuration is the complementary value of the coefficient of variation $\sigma(\vec{u})$, expressed in percent, called $\eta(\vec{u})$. This parameter takes into account the overall velocity field

$$\eta(u) = 100 - \left(\frac{s_N}{u_{mean}}\right) \cdot 100$$

where

$$s_N = \sqrt{\frac{\sum_i^N (u_i - \bar{u})^2}{N}}$$

is the standard deviation from the mean velocity in the measuring domain.

Boundary conditions

Boundary conditions are defined at the inlet of the free-flow domain, at the interface between the turbulent and porous media domain and at the wall surface.

- Inlet : constant mean velocity
- Wall : no slip
- RANS-Brinkman interface: velocity (u,v,z) vector
- Outlet : null pressure condition

Simulation Results and Discussion

Calibration of the pressure drop shows that COMSOL Multiphysics® is able to predict accurately the second order polynomial curve which describe the measured pressure drop across the heat exchanger (Figure III). The presence of the fins can be simulated accurately by suppressing the permeability components corresponding to the velocity vector normal to the flow main direction. Figure IV shows the 2D model used to calibrate the porous media and carry out the mesh refinement for pressure drop and inlet velocity profile.

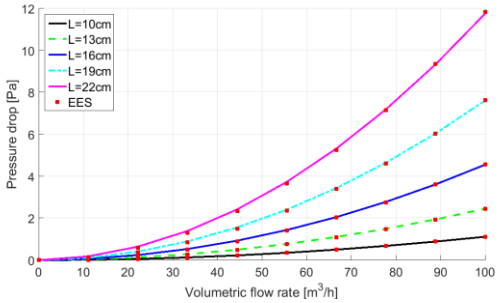

Figure III. Pressure drop curve calibration using the approach of Hooman & Gurgenci (2009); L=13 cm.

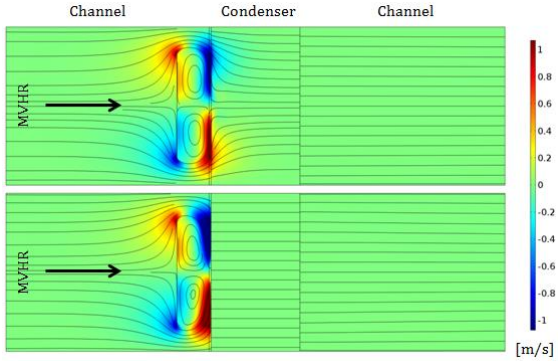

Figure IV. Flow through the heat exchanger. Normal velocity v(x,y) component suppression. Effect of the anisotropy of permeability in porous media. Top: isotropic permeability. Bottom: anisotropic permeability.

A one-dimensional obstacle is placed in front of the condenser, in order to decompose the velocity field in two components u(x,y) and v(x,y).
The images in Figure IV show the effect of porous media anisotropy on the velocity component normal to the flow direction. In the bottom image it is possible to observe its complete suppression and the rectification of streamlines within the porous media domain. Since the K_{xx} component of the K tensor is much higher than all the other ones, the v(x,y) velocity component inside the porous media domain is 0. This consideration can be extended also in three dimension. Mesh size substantially affects the velocity maldistribution in front of the condenser. By considering the difference between the maximum and minimum value of the u-velocity component magnitude (Δu), a variation of up to 40% can be observed. Moreover, by changing the discretization order, up to 10 % deviation in the velocity profile is observed.

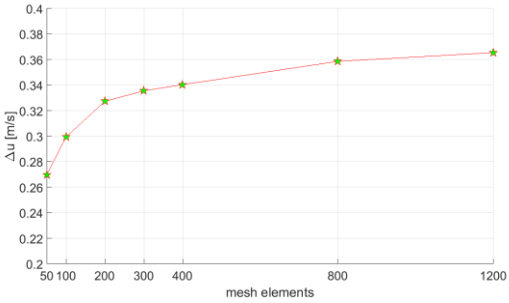

Figure V. Mesh refinement: dependency on mesh size of u-velocity component maldistribution at the inlet of the condenser.

BVM calibration

Differently from High Reynolds number models, Low Reynolds models are able to predict the transition to turbulence after the separation point, in free shear layer. This phenomenon can be observed in Figure VI.

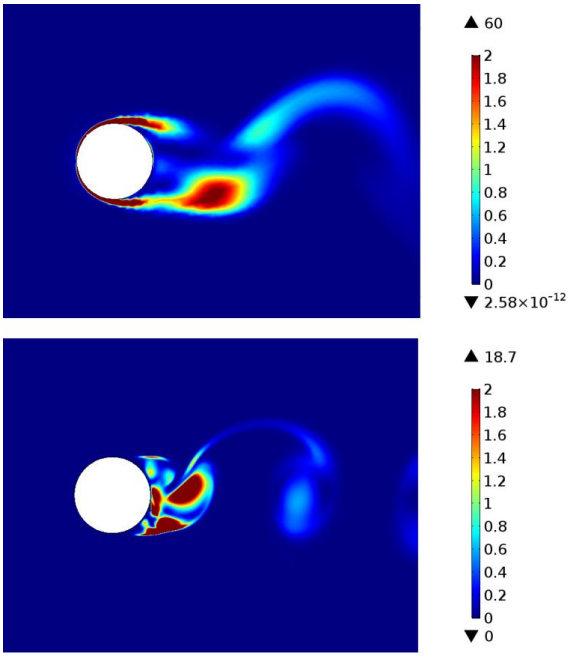

Figure VI. Instantaneous production of turbulent kinetic energy $[W/m^3]$ for standard (top) and AKN (bottom) k-ε model.

In the bottom image, the production of turbulent kinetic energy in the cylinder boundary layer is absent, while turbulence production appears behind the separation point, i.e., where the largest eddies start to extract energy from the mean flow. Shear layer transition, though, should appear between 0.7 and 1.4 diameter downstream the cylinder, due to Kelvin-Helmoltz instability. An opposite result is obtained using High Reynolds models: a consistent production of turbulent kinetic energy appears also at the stagnation point and around the cylinder boundary

layer, before the separation point. Since Wall Functions are used, at the boundary of the cylinder is possible to observe only the resolved fluid domain at a distance δ_w from the wall, and not the flow at the *real* boundary.
However, whether the model is able to account correctly for the viscous sub-layer or not, wake recirculation length is better depicted with standard k-ε model. Moreover, computational cost arises abruptly when Low Reynolds number models are used, due to the necessary near wall modelling and a general slower convergence behavior of the models.

Optimization results
Flow optimization is carried out by using stationary High Reynolds number k-ε turbulence model.

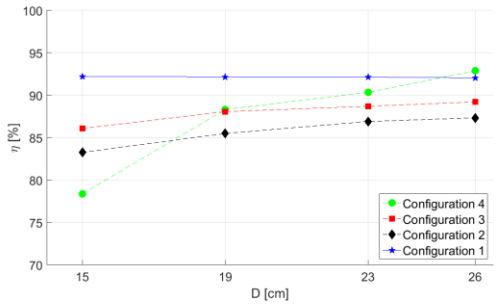

Figure VII. Flow homogeneity in front of the condenser for velocity component normal to the condenser's surface. Four different distances between the compressor and condenser centre and four configurations (Fig. II) are compared.

For every system length D, Conf. 3 gives slightly better results than Conf. 2. Concerning Conf. 4, the maldistribution is steeply improved by increasing the distance between the compressor and the condenser. This improvement may occur due to a different average distance between the compressor and the condenser inlet, and to the convergent shape of the duct, which increases the air speed around the compressor and flattens the wake structure behind it, while increasing the tip speed at the separation point (Figure VIII).
It is relevant to underline how the inlet velocity profile is affected also by anisotropy. When anisotropy is adopted in the whole condenser, a damping of the inlet velocity profile can be observed. This phenomenon derive from the two constraint that come together with anisotropy: a pressure drop characteristic within the condenser and the suppression of the velocity components v(x,y). Since at the interface of the two domains Momentum Transport Equation must be satisfied, u(x,y) and v(x,y) must adjust to this constraints. Moreover, since at the interface u(x,y) velocity component must undergo a step in its magnitude, the discretization order and mesh refinement affect the amount of elements (and space) necessary to u(x,y) to reach the value present inside the condenser. Whether anisotropy assumption holds in the whole domain or not, further studies are necessary.
Moreover, the coupling between different physical interfaces (Turbulent flow and Brinkman equations) entails the use of a Fully Coupled solver, which increases the memory requirement.

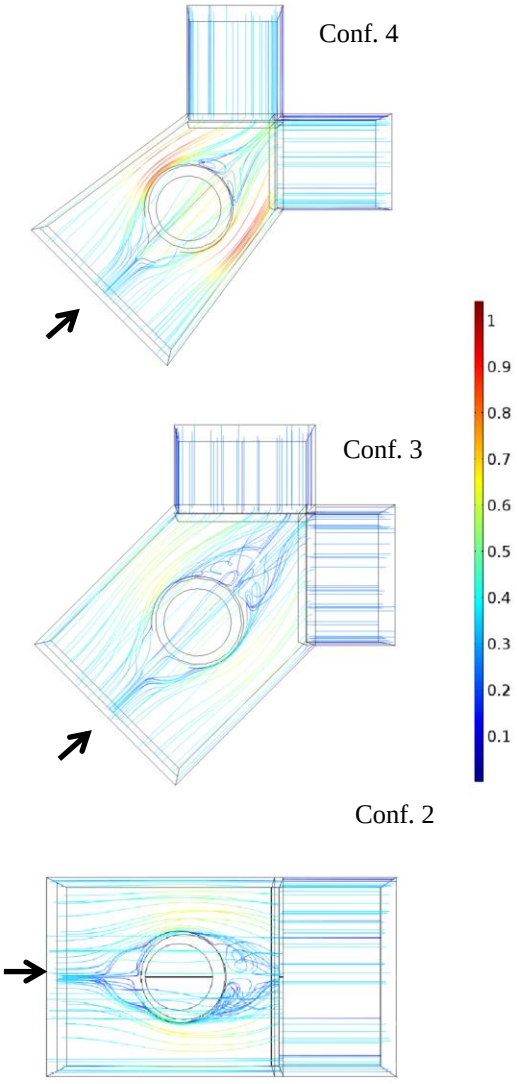

Figure VIII. Wake structure for Conf. 3,4,2. Top view for D=19 [cm]. The streamlines are coloured using velocity magnitude [m/s].

In the end, has been observed that the use of High Reynolds number turbulence models can impact consistently the wake structure. An analysis has been carried out for Configuration 2, D=26 cm. This dimension has been chosen since it is the one in which

the wake has enough space to develop. Wake structure is compared for three different turbulence models: Standard k-ε, k-ω and SST k-ω are used.
High Reynolds number models (k-ε, k-ω) show a rather symmetric wake, in which the tip trailing vortex is clearly defined and the detachment process occurs symmetrically (Figure IX).

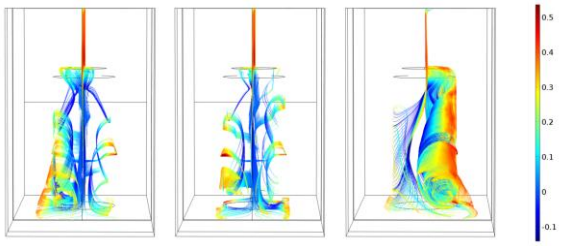

Figure IX. Downward trailing vortex: frontal view. Conf.2 D=26 [cm]. u-velocity component magnitude [m/s]. From left to right: k- ε, k-ω, SST k-ω.

Low Reynolds number model (SST k-ω) predicts an asymmetric wake structure, in which the downwash vortex detaches mainly from the lateral top edge of the compressor. This result can be explained considering that the minor turbulence damping introduced by SST k-ω might resolve better the macroscopic wake fluctuations, which are forced in this asymmetric configuration when RANS are solved in a stationary mode. However, further investigations are necessary to understand whether asymmetry arises from mesh quality, error tolerance or a general unsteady flow.

Conclusions

Turbulence models available in COMSOL might have a lack of accuracy when applied to transitional flow, and in general, Boussinesq viscosity models behave poorly in this regime. In this study, three different turbulence models (k-ε, k-ω and SST k-ω) have been considered. The SST k-ω model seems to give better results for what concerns the macroscopic wave fluctuations.
Concerning flow optimization, two sets of 90° V-styled condensers, i.e. for which the air flow is split in two different directions, have been tested. Compared to the straight condenser, a small improvement in overall flow homogeneity is observed (~ 5%). Moreover, if volume occupation is taken into account, part of the advantage is lost in one of the configurations. Pressure drop across the duct can be decreased by reducing the mean inlet velocity in the heat exchanger.

Further developments

In COMSOL®, when anisotropic porous media is employed, the coefficients of the tensor are related to the global Cartesian coordinate system of the entire model, which refer to the *spatial frame*. This limits the flexibility of the model, for example in the case in which the heat exchanger does not follow the spatial x,y,z coordinates. A solution would be to define a relative coordinate system related to the porous media domain inlet, by employing a Base Vector System and use it with Curvilinear Coordinates interface. However, for the moment it is not possible to implement this solution in COMSOL®.

ACKNOWLDEGEMENT

This work is part of the Austrian research project SaLüH! Renovation of multi-family houses with small apartments, low-cost technical solutions for ventilation, heating & hot water (2015-18); Förderprogramm Stadt der Zukunft, FFG, Project number: 850085.

Acronyms

CFD: Computational Fluid Dynamic
MVHR: mechanical ventilation heat recovery
EES: Engineering equation solver
AKN: Abe- Kondoh-Nagano
SST: Shear-stress transport
BVM: Boussinesq Viscosity Models

References

1. Marco Romani, *Flow Optimization of a MVHR combined with an Exhaust air Heat Pump by means of CFD Simulation*, Master Thesis, Termotecnica e impianti termotecnici, Alma Mater Studiorum – Universitá di Bologna, Bologna, (2016)
2. P. Beaudan and P. Moin, "Numerical experiments on the flow past a circular cylinder at sub-critical Reynolds number," *Stanford University*, 1994.
3. A. Bhutta and A. R. Khan, "CFD applications in various heat exchangers design: A review," *Applied Thermal Engineering*, 2011.
4. F. Ochs, D. Siegele, G. Dermentzis and W. Feist, "Prefabricated Timber Frame Façade with Integrated Active components for Minimal Invasive Renovation," *Energy Procedia*, pp. 61-66, 2015.
5. K. Vafai, Handbook of Porous Media, Basel: Marcel Dekker , 2000.
6. M. Musto, N. Bianco, G. Rotondo, F. Toscano and G. Pezzella, "A simplified methodology to simulate a heat exchanger in an aircraft's oil cooler by means of a Porous Media model," *Applied Thermal Engineering*, pp. 836-845, 2015.
7. COMSOL, COMSOL CFD: User's Guide (v5.2), 2015.
8. iNSPiRe http://inspirefp7.eu/
9. SaLüH! https://www.uibk.ac.at/bauphysik/forschung/projects/saluh/index.html.de